

Investigation of DFMs for CO₂ Capture and Methanation by Coupled Microreactor Experiments and FT-IR Spectroscopy

Alessandro Porta, Roberto Matarrese, Carlo Giorgio Visconti, and Luca Lietti*



Cite This: *Energy Fuels* 2023, 37, 7280–7290



Read Online

ACCESS |



Metrics & More

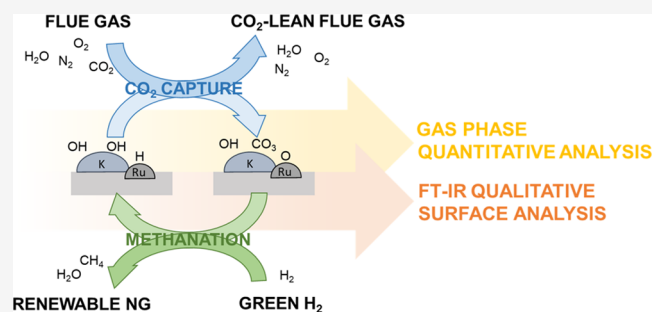


Article Recommendations



Supporting Information

ABSTRACT: In this work, we discuss the role of different atmospheres and process conditions on the catalytic performances of Ru- and K/Ba-based dual-function materials (DFMs) for CO₂ capture and methanation. By a combination of microreactor experiments and Fourier transform infrared (FT-IR) spectroscopy, we clarify the effect of temperature and H₂ partial pressure during the hydrogenation step and the effect of water and oxygen during the CO₂ adsorption step. In particular, we show that between 250 and 400 °C CO₂ is rapidly adsorbed as bidentate carbonates on the basic sites (K or Ba) and as CO on Ru metal surfaces with decreasing storage capacity with increasing temperature. Increasing the operating temperature and the H₂ partial pressure, the methanation rate of the bidentate carbonates increases. We also show that during the CO₂ capture step, water not only reduces the amount of CO₂ adsorbed by competitively adsorbing on basic sites but also changes the nature of the adsorbed carbonates, increasing their ionic character and hence their stability. This is observed in the case of both a K-based DFM and a Ba-based DFM, though in the case of the alkaline earth, the phenomenon is more evident. Finally, we point out that the presence of O₂ during the CO₂ capture step removes metallic Ru as CO adsorption site and reduces the amount of bidentate carbonates, possibly due to the additional presence of water formed upon Ru reduction in the methanation step. The information presented in this work is of interest to improve the design of DFMs to be used for flue gas, where the partial pressure of water and oxygen is relevant.



1. INTRODUCTION

CO₂ emissions associated with human activities have been widely recognized by the scientific community as the major source of the ongoing climate change. The need to take urgent action to face this threat has stimulated the development of new materials and methods for postcombustion CO₂ capture technology.

An innovative abatement strategy for carbon neutral power generation is based on the exploitation of dual-function materials (DFMs) for cyclic CO₂ capture and methanation,^{1,2} a technology combining the CO₂ capture step and its hydrogenation to methane in a single catalytic reactor. In a typical cycle, CO₂ is stored on the DFM upon contact with a CO₂-rich stream (adsorption step); the adsorbed CO₂ is then transformed into methane upon reaction with H₂ (hydrogenation step). In DFM formulations, an alkaline or alkaline earth CO₂ adsorbent phase (typically Na or Ca) and a metal active for the CO₂ methanation reaction (typically Ru and/or Ni) are dispersed over a high-surface-area, nonreducible support.^{3–5} The coupling of adsorption and reduction capabilities in a single solid allows us to avoid the energy-intensive thermal or pressure swing that is usually requested in the CO₂ capture/release cycle to regenerate the adsorbent.^{5–7} In fact, in the case of DFM, the thermal input required for CO₂

release from the storage sites is supplied by the exothermic methanation reaction.

As demonstrated in previous studies, during cyclic tests, CO₂ is mainly adsorbed on the DFM alkaline sites as bidentate carbonates on both alkaline and alkaline-earth metals.^{8–10} Some CO₂ could also react during the adsorption phase—possibly using residual hydrogen left on the DFM surface from the hydrogenation phase of the previous cycle—to form CO on Ru surfaces.^{9–11} Upon exposure of the catalyst to H₂, the adsorbed CO₂ is converted into CH₄ with the intermediacy of carbonyls and possibly formates,^{8,9,12,13} in agreement with the mechanisms proposed for conventional CO₂ methanation.^{14,15}

Most of literature data on DFMs are available under ideal conditions, i.e., with the CO₂ capture step carried out in the absence of O₂ and H₂O in the feed.^{3,6} However, these two species are both present in the case of flue gas and direct air capture (DAC) application. Proaño et al. investigated the effect

Received: February 16, 2023

Revised: April 20, 2023

Published: May 1, 2023



of O₂ presence during the capture phase over DFMs using diffuse reflectance infrared Fourier transform spectroscopy (DRIFTS) and concluded that the carbonate species on the storage component of the DFM are not affected by O₂ presence; however, some storage capacity in these conditions may be lost due to the oxidation of the methanation active metal on the DFM.¹⁶ Indeed, while in O₂-free conditions, the methanation active metal provides additional storage sites where CO₂ is reduced and adsorbed as CO during the capture step; in the presence of O₂, the sites are oxidized and unable to reduce CO₂.¹⁷ During the hydrogenation step following the capture in an oxidative environment, the methanation active element has to be reduced to be catalytically active in the methanation reaction. This is reasonably easy for noble metals such as Ru, while oxidized Ni cannot be efficiently reduced in the DFM operating window of 250–350 °C.^{18,19} The redox properties of Ni-based DFM can be improved to some extent by noble metal doping, but nevertheless, since high Ni loadings are required to achieve reasonable methanation capacity, the high exothermicity of the catalyst reduction and oxidation hinders the adsorption/methanation process even at the laboratory scale.²⁰

The effect of water is less investigated, and normally, cyclic tests are carried out in the presence of both O₂ and H₂O during the adsorption feed. It is generally accepted that in flue gas application H₂O competitively adsorbs onto the alkali sites of the DFM, decreasing CO₂ adsorption capacity.^{9,10} For DAC applications, an increase of the CO₂ storage capacity at room temperature is observed in the presence of moisture on Na-based DFM, possibly due to the restructuring of Na allowing the formation of bicarbonate species at the investigated conditions.²¹

On these bases, starting from what we reported in a recent publication⁹ where we compare the behavior of different alkaline materials and provide spectroscopic information on the CO₂ storage-reduction behavior of Ba- and K-based DFMs, the aim of this work is to deepen the understanding of the effect of operating conditions and in particular of the presence of O₂ and H₂O on the behavior of a K-based DFM. In particular, by coupling microreactor experiments and in situ FT-IR characterization to get a comprehensive description of the storage-reduction behavior and on the effect of oxygen and water, in this work, we discuss the effect of different operating conditions and feed composition on a K-based DFM. Selected operating conditions are also investigated using a Ba-based DFM to provide a comparison of the two different DFM formulations.

2. EXPERIMENTAL SECTION

2.1. Catalyst Preparation. The DFMs used in this work were prepared starting from a commercial γ -Al₂O₃ (Sasol Puralox, 75–105 μ m, S_{BET} = 191 m²/g, V_p = 0.5 cm³/g). The support was impregnated (incipient wetness impregnation) with a Ru(NO)(NO₃)₃ solution (Alfa Aesar, 1.5% g_{Ru}/mL) to obtain a Ru loading of 1% by weight. The nitrate precursor was then decomposed in a H₂ flow at 400 °C for 3 h (heating rate: 2 °C/min), cooled down to room temperature in inert, and then treated with a diluted oxygen flow (2% O₂/He, 1 L(STP)/h/g). The passivated sample was then impregnated with a CH₃COOK solution (prepared from the anhydrous salt, Sigma-Aldrich >99%) to obtain a nominal K-loading of 5% by weight of the final Ru–K/Al₂O₃ DFM (indicated as RuK/Al in the following). Alternatively, the passivated Ru/Al₂O₃ sample was impregnated with a (CH₃COO)₂Ba solution (prepared also in this case from the anhydrous salt, Sigma-Aldrich >99%) to obtain a nominal Ba-loading

of 16% by weight of the final Ru–Ba/Al₂O₃ sample (RuBa/Al). After the impregnation step with the acetate salt, the DFMs were dried overnight at 120 °C in static air and stored as such. Additional information on the preparation and characterization of the materials is available elsewhere.⁹

2.2. Microreactor Experiments. Microreactor experiments were carried out over 60 mg of dried sample (75–105 μ m) placed in a quartz reactor (I.D. = 8 mm). The temperature of the catalytic bed is monitored using a K-type thermocouple placed on the reactor axis at the center of the catalytic bed. A constant inlet flowrate of 100 mL (STP)/min was used in all tests (corresponding to a GHSV of 100 L(STP)/h/g), using two 4-way valves to ensure fast and reproducible changes in the feed composition. The effluents were monitored with three different analyzers: Pfeiffer QMS200 mass spectrometer (to follow H₂ – m/z = 2, CH₄ – m/z = 15, H₂O – m/z = 18, CO – m/z = 28, O₂ – m/z = 32, Ar – m/z = 40, CO₂ – m/z = 44; measure every 4 s), an Agilent 3000 micro gas chromatograph (to follow CH₄, CO, CO₂; measure every 180 s), and an MKS Multigas 2030 FT-IR spectrometer (to follow CH₄, H₂O, CO, CO₂; measure every 0.9 s). Additional information about the microreactor experimental setup can be found in our previous paper.¹¹

Before running the catalyst reactivity test, the acetate precursor is decomposed in situ at 500 °C in an inert flow (heating rate: 10 °C/min), cooled down to 100 °C, and then reduced in diluted H₂ flow (4% H₂/He) at 500 °C (heating rate: 10 °C/min). The effluents were monitored during both temperature ramps and indicated the complete decomposition of the acetate precursor, possibly leading to the formation of carbonates and oxides/hydroxide species on the catalyst surface.⁹

After the reduction, CO₂ capture and methanation cycles under different operating conditions were carried out. Each cycle involves a 10 min CO₂ capture step (1% CO₂/He) and a 10 min hydrogenation step (0.4–4% vol% H₂/He), spaced out by an inert purge (5 min). A set of three consecutive cycles were repeated to obtain reproducible results; results discussed in this work refer to the last cycle of the set. After each cycle set, the sample was heated in 4% H₂/He to 500 °C (heating rate: 10 °C/min) to sweep the catalyst surface.

Initially, we investigated the effect of temperature, performing cycles in the range of 250–400 °C. Then, the effect of the partial pressure of H₂ during the methanation step was probed by performing cycles at different H₂ concentrations in the range of 0.4–4% (see Figure S1A in the Supporting Information for the graphical representation of the microreactor tests).

The effect of water during the capture step was investigated by feeding 2.5% of H₂O using a water saturator kept at the desired temperature. Besides the base case (Figure S1A), three different conditions were looked into: (i) cofeeding of H₂O and CO₂ (Figure S1B); (ii) exposure to H₂O before CO₂ capture (Figure S1C); and (iii) exposure to H₂O after CO₂ capture (Figure S1D). In particular, in case (i), water was admitted during the purge step, 2 min prior to CO₂ admission, and removed 2 min after CO₂ removal, whereas in cases (ii) and (iii), an additional 10 min “H₂O adsorption” step (followed by a 5 min purge) was added to each cycle.

At last, the effect of O₂ in the presence/absence of 2.5% of H₂O was investigated by simultaneously cofeeding 3% of O₂ and CO₂ during the capture step (see Figure S2 in the Supporting Information for the graphical representation of the experimental procedure).

Quantitative amounts of CH₄ and CO during the hydrogenation step are evaluated by integrating the concentration signals vs time. Given the relatively high amount of CO₂ fed, it is difficult to precisely evaluate the CO₂ storage capacity from the adsorption pulse. Hence, the “CO₂ storage capacity” is calculated as the sum of the CH₄ and CO evolving during the hydrogenation step of the cycle and the CH₄ and CO evolving during the final heating in H₂ to 500 °C. This amount likely underestimates the total amount of CO₂ present on the DFM, as strongly bound species may be retained onto the sample even at 500 °C in the presence of H₂.⁶ The third capture/hydrogenation cycle and the subsequent heating in H₂ to 500 °C are shown in Figure S3, highlighting the contributions used to

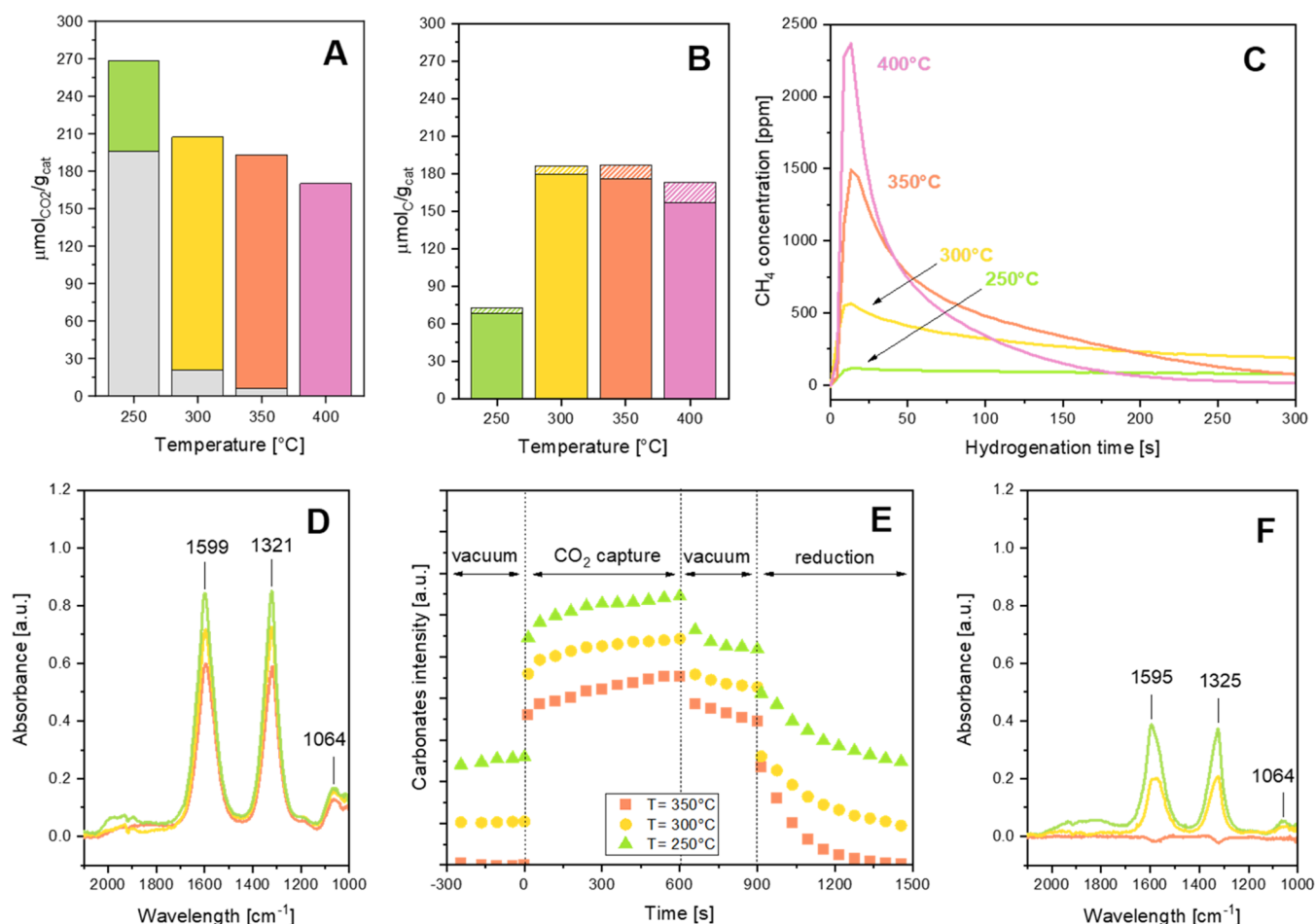


Figure 1. Temperature effect on CO₂ capture/methanation cycles by microreactor experiments (A–C) and in situ FT-IR (D–F) on the Ru–K DFM. (A) Total CO₂ adsorbed during the capture step (total height), composed by a fraction that is hydrogenated at the same temperature of adsorption (colored bar) and by a fraction evolved only during heating (gray portion); (B) CH₄ (solid) and CO (dashed) produced during the hydrogenation step of the third cycle; (C) CH₄ evolution during the first 300 s of the hydrogenation step of the third cycle; (D) spectra at the end of the capture step ($t = 600$ s in panel (E)); (E) qualitative evolution of carbonate bands during capture/hydrogenation cycles; (F) spectra at the end of the hydrogenation step ($t = 1500$ s in panel (E)). Operating conditions, microreactor: adsorption: 1% CO₂/He, 10 min; hydrogenation: 4% H₂/He, 10 min. Operating conditions, FT-IR: adsorption: 5 mbar CO₂, 10 min; hydrogenation: 40 mbar H₂, 10 min.

evaluate the corresponding amounts of stored CO₂ and C-containing products evolving during the hydrogenation step.

Notably, this method allows the distinction between CO₂ adspecies that are cyclically involved in the methanation at a fixed temperature and the overall amounts of CO₂ stored on the catalyst.

2.3. FT-IR Experiments. In situ transmission FT-IR characterization was carried out using a Nicolet Nexus Fourier transform instrument with a DTGS detector (resolution = 4 cm⁻¹, number of scans = 20). About 15 mg of sample was grounded, pressed in a self-supporting wafer of 1.3 cm diameter, and inserted in a stainless steel cell (ISRI Infrared Reactor, Granger, IN). CO₂ capture/hydrogenation cycles were performed in a controlled atmosphere by adjusting the partial pressure of the different species to obtain conditions similar to those used for microreactor experiments.

Before all measurements, the sample was pretreated at the maximum temperature of 375 °C in H₂ (100 mbar).⁹ The temperature was limited to 375 °C to ensure the reliability of the vacuum seal of the FT-IR cell. CO₂ capture and methanation cycles were performed by alternating CO₂ (1–5 mbar, 10 min) and H₂ (10–100 mbar, 10 min) atmospheres at 350 °C, separated by a vacuum purge (5 min). As done in the case of microreactor experiments, also in this case, three consecutive cycles were repeated in each condition to ensure the good reproducibility of the results (Supporting Information, Figure S4A). The effects of the presence of H₂O vapor (25 mbar) and O₂ (30 mbar) at 350 °C were also addressed;

water effect was investigated by exposing the sample to 25 mbar of H₂O vapor (10 min) during, before, or after the CO₂ capture step (Figure S4), while oxygen was added with CO₂ (Figure S5). Water vapor was added by applying vacuum to a round-bottom flask filled with deionized water, causing the water to boil and generating vapor up to the saturation pressure at ambient temperature. The vapor was then dosed to the FT-IR cell where the DFM wafer was located.

In all FT-IR experiments, the spectral features corresponding to the gas-phase species (e.g., CO and CH₄) could not be observed due to their low concentration.

In the figures of this work, FT-IR spectra are shown as difference spectra, where the subtrahend spectrum is that of the clean sample after the activation in H₂. To appreciate better the trend of the adsorbed species with the progression of the test, the carbonate bands were integrated into the range of 1750–1200 cm⁻¹ for each spectrum and reported as “carbonates integrated intensity” as a function of time.

3. RESULTS AND DISCUSSION

3.1. Temperature Effect. At first, we investigated the effect of temperature during CO₂ capture and methanation cycles (Figure 1). Figure 1A shows the effect of temperature on the CO₂ storage capacity. As previously indicated, this quantity is estimated from the sum of products evolved during hydrogenation of the stored CO₂ (carried out at the adsorption

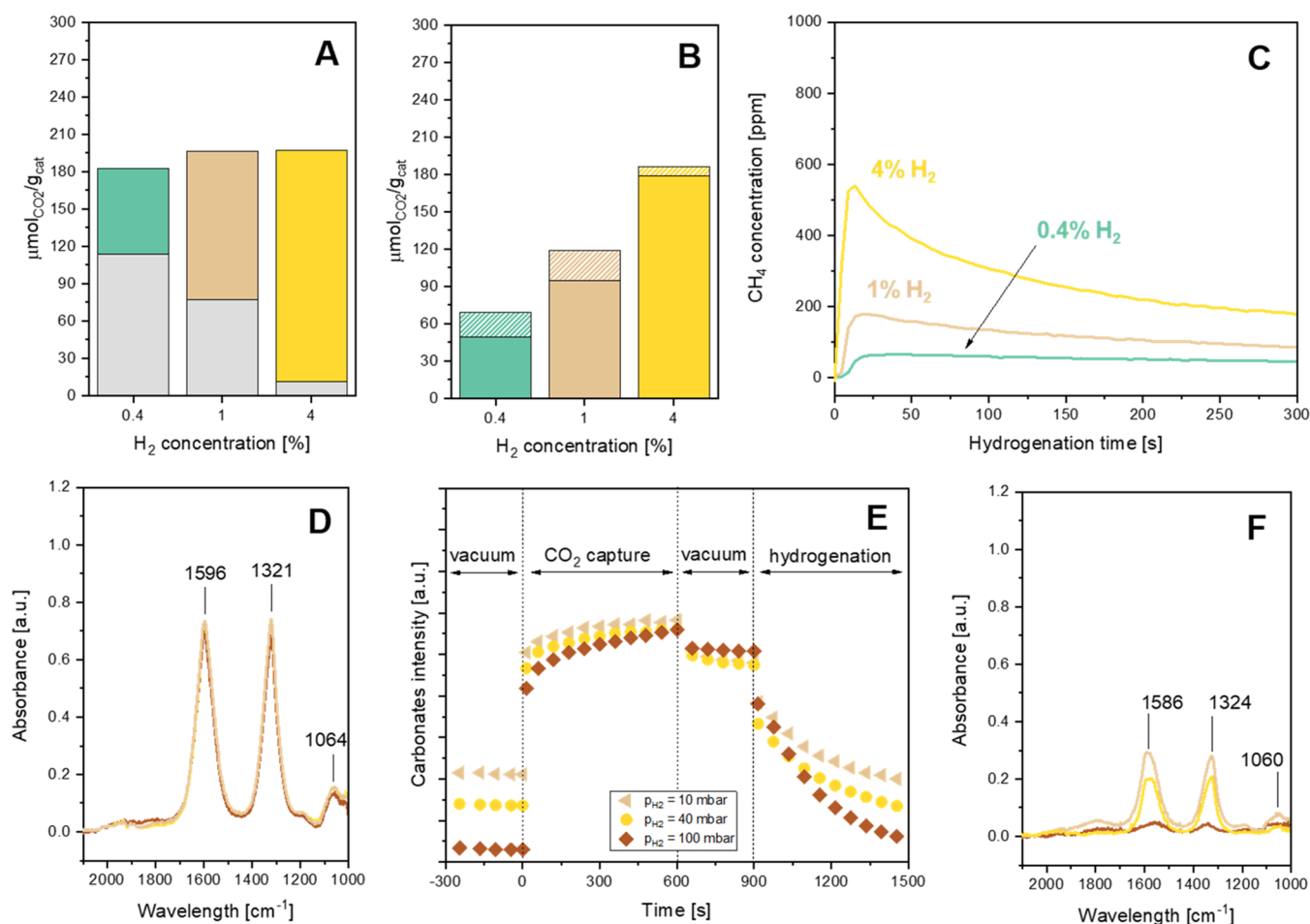


Figure 2. H₂ partial pressure effect on CO₂ capture/methanation cycles by microreactor experiments (A–C) and in situ FT-IR (D–F) at a fixed temperature of 300 °C on the Ru–K DFM. (A) Total CO₂ adsorbed during the capture step (total height), composed by a fraction that is hydrogenated at the same temperature of adsorption (colored bar) and by a fraction evolved only during heating (gray portion); (B) CH₄ (solid) and CO (dashed) produced during the hydrogenation step; (C) CH₄ evolution during the first 300 s of the hydrogenation step of the third cycle; (D) spectra at the end of the capture step ($t = 600$ s in panel (E)); (E) qualitative evolution of carbonate bands during capture/hydrogenation cycles; (F) spectra at the end of the hydrogenation step ($t = 1500$ s in panel (E)). Operating conditions, microreactor: adsorption: 1% CO₂/He, 10 min; hydrogenation: 0.4–4% H₂/He, 10 min. Operating conditions, FT-IR: adsorption: 5 mbar CO₂, 10 min; hydrogenation: 10–100 mbar H₂, 10 min.

temperature) and products released upon heating the catalyst under H₂ at 500 °C. Note that Table S1 of the Supporting Information reports all results shown in figures As and Bs of this article.

As expected, the CO₂ storage capacity decreases with increasing temperature due to the exothermic nature of the adsorption process. Besides, it clearly appears that the fraction of adsorbed CO₂ that is hydrogenated at the adsorption temperature (colored bar) increases with temperature, as expected due to kinetic reasons.

The reduction products evolved during the cycle are plotted in Figure 1B, distinguishing between CH₄ and CO. A maximum is observed in CH₄ evolution, peaking at 300–350 °C, due to the trade-off between the amount of CO₂ adsorbed—favored at low temperature (Figure 1A)—and the CH₄ formation rates—kinetically favored at high temperatures. Increasing amounts of CO are observed with increasing temperatures, in line with the thermodynamics of CO formation via reversed water gas shift reaction. Similar trends for CO₂, CO, and CH₄ have been reported also in the case of Ni-based DFMs in comparable conditions, though in this case,

the maximum CH₄ production was observed at higher temperatures,²² possibly due to the lower methanation turnover frequency on Ni with respect to Ru.^{23,24}

Figure 1C shows the CH₄ evolution profile during the first 300 s after H₂ admission. At the lowest investigated temperature (250 °C), CH₄ formation is slow, resulting in a low and steady CH₄ concentration in the effluents. As the temperature increases, CH₄ evolution becomes more pronounced at the beginning of the hydrogenation phase, where a sharp peak is observed, tailing down with time. Above 350 °C, CH₄ production is very fast and concentrated in the first 100 s of the hydrogenation step: in these conditions, the methanation kinetics is very fast and rapidly consumes all of the available adsorbed CO₂ at the DFM surface. As a consequence, at these temperatures, the integral amount of C-containing reduction products during a single cycle matches the amount of stored CO₂ in the same cycle (see Figure 1A,B), and accordingly, no product evolution is observed during the heating in H₂ after the cycle set (indicated by the absence of the gray portion of the pink bar at 400 °C in Figure 1A).

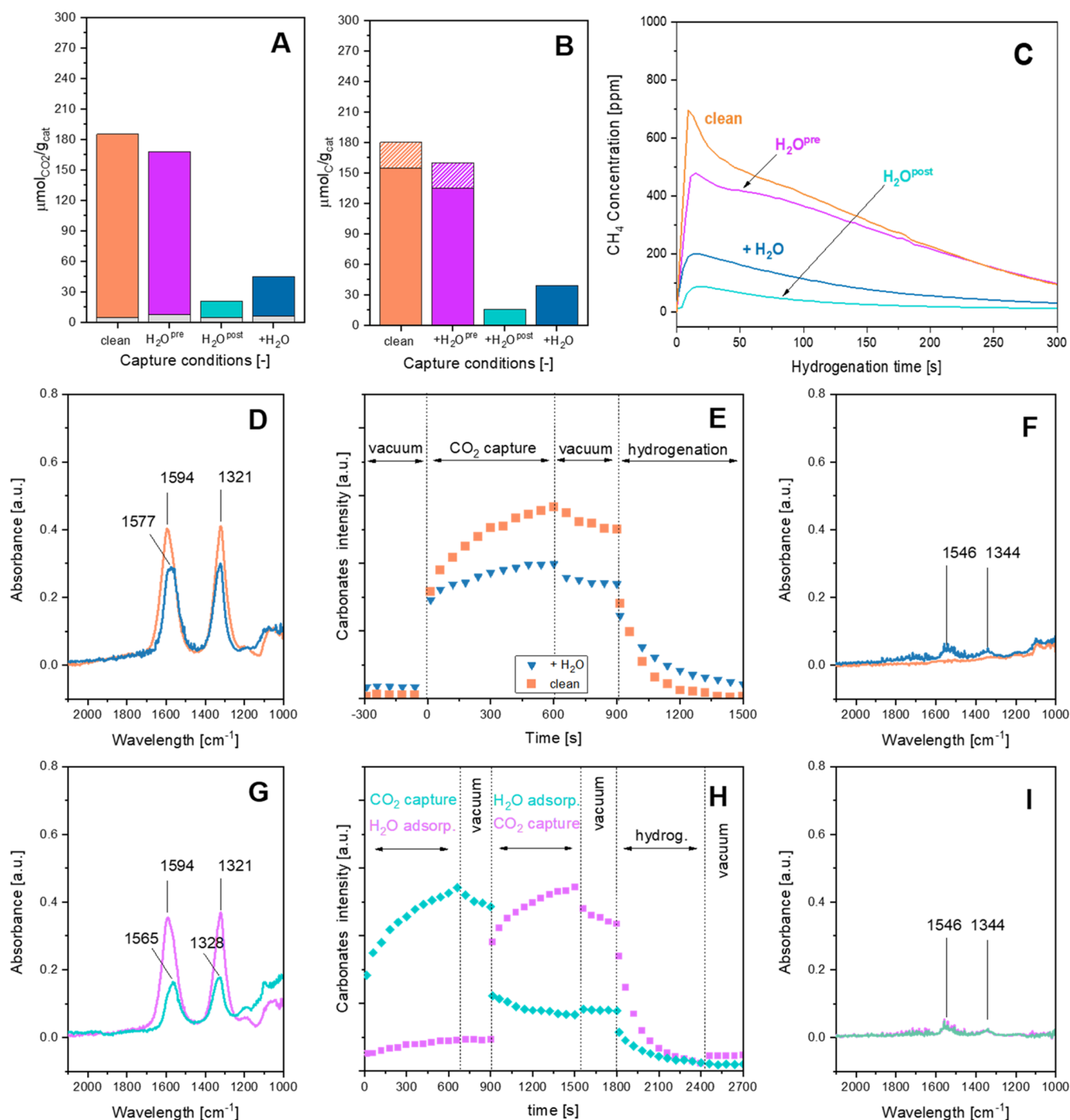


Figure 3. Effect of H₂O presence on CO₂ capture/methanation cycles by microreactor experiments (A–C) and in situ FT-IR (D–I) at a fixed temperature of 350 °C on the Ru–K DFM. (A) Total CO₂ adsorbed during the capture step (total height), composed by a fraction that is hydrogenated at the same temperature of adsorption (colored bar) and by a fraction evolved only during heating (gray portion); (B) CH₄ (solid) and CO (dashed) produced during the hydrogenation step; (C) CH₄ evolution during the first 300 s of the hydrogenation step; (D) spectra at the end of the capture step ($t = 600$ s in panel (E)); (E) qualitative evolution of carbonate bands during capture/hydrogenation cycles in the reference case and with cofed H₂O during the capture step; (F) spectra at the end of the hydrogenation step ($t = 1500$ s in panel (E)); (G) spectra at the end of the capture steps ($t = 1800$ s in panel (H)); (H) qualitative evolution of carbonate bands during capture/hydrogenation cycles with the additional H₂O adsorption step; (I) spectra at the end of the hydrogenation step ($t = 2400$ s in panel (H)). Operating conditions, microreactor: adsorption: 1% CO₂/2.5% H₂O/He, 10 min; hydrogenation: 4% H₂/He, 10 min. Operating conditions, FT-IR: adsorption: 1 mbar CO₂/25 mbar H₂O, 10 min; hydrogenation: 40 mbar H₂, 10 min.

The reduction is very selective to methane since only minor amounts of CO are observed during the hydrogenation step (see Figure 1B). CO is seen as a small peak only at the very beginning of the hydrogenation step (not shown in Figure 1C).

This likely arises from CO formed on Ru surfaces toward the end of the catalytic bed; these species are desorbed as a result of the local temperature increase of the DFM and are not efficiently readsorbed and hydrogenated to CH₄.

Concerning the adsorbed species, regardless of the adsorption temperature, CO₂ exposure results in adsorption bands centered at 1599, 1321, and 1064 cm⁻¹, characteristic of surface bidentate carbonate species on the alkaline phase (Figure 1D).^{25,26} In addition, the wide envelope in the range of 2000–1800 cm⁻¹ is related to the minor formation of carbonyl species on Ru surfaces.^{27,28}

The integrated values of the carbonate peaks during a representative cycle at the investigated temperatures are shown in Figure 1E. Before the CO₂ adsorption, residual carbonates from previous cycles at the same temperature are already present on the DFM surface at 300 and 250 °C (Figure 1E; $t < 0$ s). During the capture step (Figure 1E; $t = 0$ –600 s), carbonate bands increase quickly in the first 50 s and then slowly increase until the end of the adsorption step. A similar adsorption dynamic—though on a longer time scale—has been observed during thermogravimetric analysis (TGA) tests in similar adsorption conditions for DAC applications.²⁹ This result confirms that in the investigated temperature range CO₂ is adsorbed fast at the very beginning of the capture step to reach almost the saturation point of the DFM, while a minor amount is adsorbed during the rest of the capture step, likely due to the formation of weakly adsorbed carbonates. In fact, during the vacuum purge step (Figure 1E; $t = 600$ –900 s), the carbonate intensity decreases and reaches a very similar value to that obtained at the beginning of the adsorption step. These data agree with the gas-phase results, where lower temperatures allow a higher amount of adsorbed CO₂ on the DFM surface.

Focusing on the carbonate dynamic during the hydrogenation step (Figure 1E; $t = 900$ –1500 s), it is evident that carbonates are slowly converted to CH₄ at 250 °C, with a considerable amount of residual adsorbed species at the end of the hydrogenation step. At variance, at 350 °C, the carbonate consumption profile is steeper, with the complete removal of all of the CO₂ adsorbed on the DFM at the end of the hydrogenation phase (Figure 1F), in agreement with the gas-phase results. Carbonyls, reaction intermediates in the CO₂ methanation reaction, are observed during the hydrogenation step at all investigated temperatures. As more extensively detailed in one of our previous works,⁹ carbonyls go through a maximum at the beginning of the hydrogenation step and are progressively consumed as the hydrogenation time proceeds. As observed in the case of carbonates, at low temperatures, the reduction kinetics is slow, and residual carbonyls can still be observed on the DFM surface at the end of the hydrogenation phase (Figure 1F; envelope at 2000–1800 cm⁻¹).

3.2. H₂ Partial Pressure Effect. Figure 2 shows the effect of the H₂ partial pressure in the hydrogenation step during CO₂ capture and methanation cycles at 300 °C. As expected, the overall CO₂ storage capacity is not affected by the H₂ partial pressure of the previous hydrogenation step of the cycle (Figure 2A); at variance, a clear change in the amounts of reducible and not reducible CO₂ at 300 °C (colored and gray bars, respectively) is well evident. In fact, a promoting effect is observed on CH₄ production at increasing H₂ concentration (Figure 2B). This is in line with the high dependency of conventional CO₂ methanation kinetics on H₂ partial pressures.^{30,31} As a result, by looking at the CH₄ evolution profiles during the hydrogenation step (Figure 2C), increasing the H₂ concentration results in a faster CH₄ production.

By increasing the H₂ concentration at constant temperature, a positive decrease in CO production is also observed as

increasing partial pressure of H₂ favors the CH₄ selectivity (Figure 2B).

Moving to the adsorbed species, the carbonates formed during the adsorption phase (Figure 2E; $t = 0$ –600 s) show a very fast increase when CO₂ is admitted and then a slower increase at higher CO₂ exposure times. At the end of the adsorption, the intensity of the adsorbed carbonates is very similar in all investigated conditions, in agreement with the substantial equivalence in the amount of stored CO₂ observed from the gas-phase results (Figure 2D). During the hydrogenation step, the rate of carbonate consumption increases with the H₂ partial pressure (Figure 2E), resulting in lower carbonate intensity at the end of the hydrogenation step (Figure 2F). This trend well replicates the microreactor experimental results shown in Figure 2A, where the gray bar indicates the amounts of residual CO₂ left on the DFM at the end of the hydrogenation phase and removed from the sample only during the final heating at 500 °C.

3.3. H₂O Effect. As detailed in the Experimental Section and further detailed in Figure S1 of the Supporting Information, the effect of water during capture/methanation cycles has been investigated by adsorbing CO₂ in the presence of water (indicated throughout the text and figures with the notation “+H₂O”, although water presence was maintained 2 min after CO₂ removal in the case of microreactor experiments), after water adsorption (“+H₂O^{pre}”) or before water (“+H₂O^{post}”).

Figure 3A shows the results, in terms of the total adsorbed CO₂, obtained from the microreactor experiment in various conditions. Comparing the amounts measured in the absence of water with those measured in the presence of water cofeed (orange and blue bars, respectively), it appears that the presence of water during the adsorption phase (and for 2 min after the CO₂ closure) significantly depresses the CO₂ storage capacity. As a consequence, the amount of produced methane is very small (Figure 3B,C). Also, no CO formation is observed. We speculate that the absence of CO may be related to the lower CO₂ adsorbed on the DFM in the presence of H₂O, causing an increase in the surface H/C ratio during the hydrogenation step and consequently promoting CH₄ selectivity.

When CO₂ is stored after H₂O adsorption (Figure 3A–C, in purple), the CO₂ storage capacity is similar to that measured under water-free conditions and also the amount of CH₄ and CO formed are comparable, indicating that in this case the storage/reduction behavior is not affected. At variance, when H₂O is fed after the CO₂ adsorption step (Figure 3A, in green), the amount of CO₂ adsorbed drops, resulting in values lower but comparable to those obtained in the case of the cofeeding tests. During the hydrogenation, the adsorbed CO₂ is completely converted to CH₄, with no CO formation (Figure 3B,C).

The concentration in the effluents during the “+H₂O^{pre}” and “+H₂O^{post}” experiments is shown in the Supporting Information, Figure S6. Figure S6A shows that as soon as water is fed to the CO₂-saturated DFM (“+H₂O^{post}”), CO₂ is released in the gas phase. In the same way, when CO₂ is fed to the water-saturated DFM (“+H₂O^{pre}”), water is released from the DFM (Figure S6B). This clearly indicates the competitive adsorption of CO₂ and water for the same adsorption sites of the DFM.

The results of the corresponding tests carried out in the FT-IR setup are shown in panels (D–I) of Figure 3 (see also Figure S4 of the Supporting Information for experimental

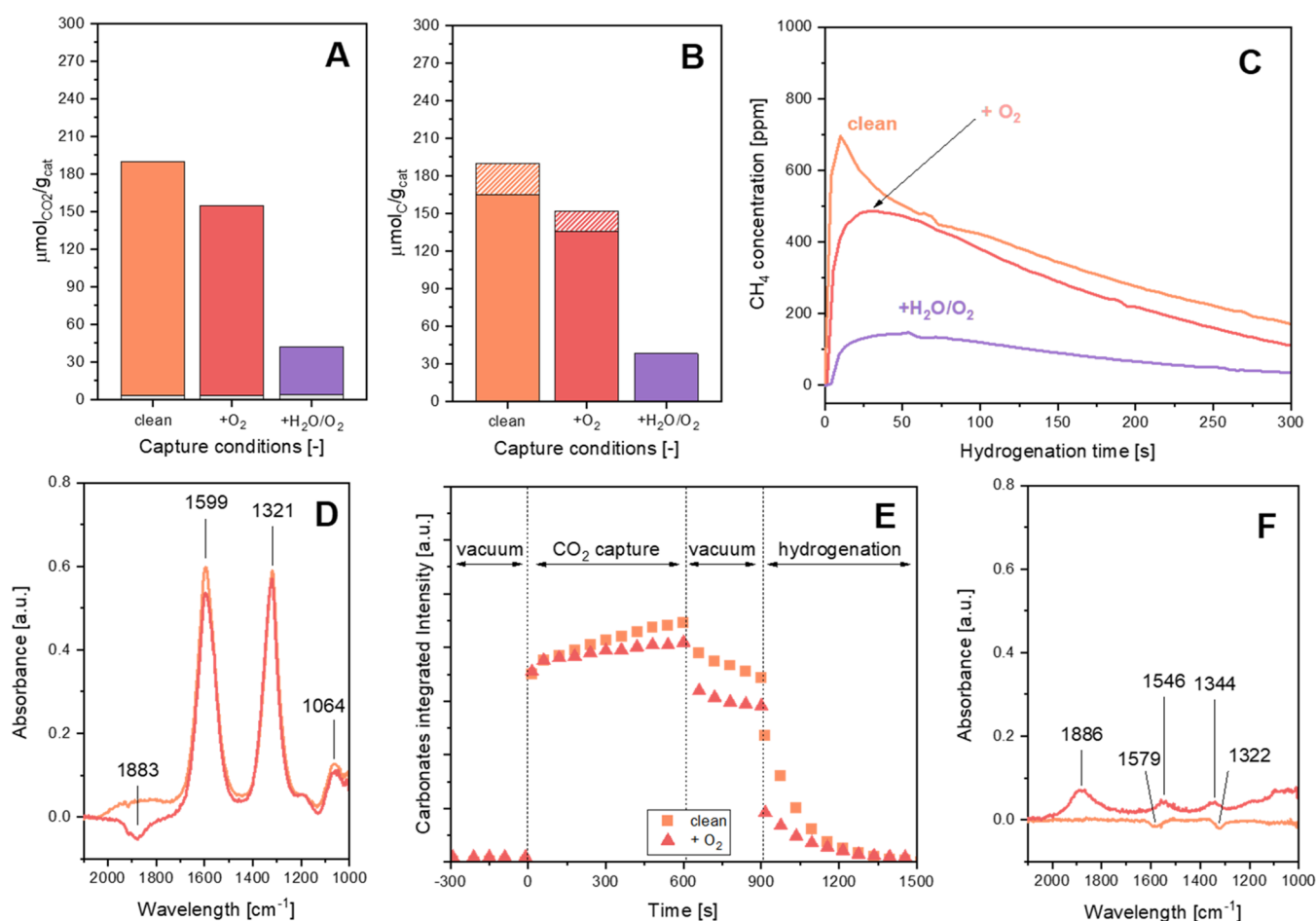


Figure 4. O₂ effect on CO₂ capture/methanation cycles by microreactor experiments (A–C) and in situ FT-IR (D–F) at a fixed temperature of 350 °C on the Ru–K DFM. (A) Total CO₂ adsorbed during the capture step (total height), composed by a fraction that is hydrogenated at the same temperature of adsorption (colored bar) and by a fraction evolved only during heating (gray portion); (B) CH₄ (solid) and CO (dashed) produced during the hydrogenation step; (C) CH₄ evolution during the first 300 s of the hydrogenation step of the third cycle; (D) spectra at the end of the capture step ($t = 600$ s in panel (E)); (E) qualitative evolution of carbonate bands during capture/hydrogenation cycles; (F) spectra at the end of the hydrogenation step ($t = 1500$ s in panel (E)). Operating conditions, microreactor: adsorption: 1% CO₂/3% O₂/2.5% H₂O/He, 10 min; hydrogenation: 4% H₂/He, 10 min. Operating conditions, FT-IR: adsorption: 5 mbar CO₂/30 mbar O₂, 10 min; hydrogenation: 40 mbar H₂, 10 min.

details). In particular, Figure 3D–F shows a comparison of the results obtained under water-free conditions and cofeeding H₂O vapor during the CO₂ capture phase, whereas Figure 3G–I shows the results obtained when H₂O was fed before and after the CO₂ adsorption step, purple and light blue signals, respectively.

In the presence of cofed water, bidentate carbonates are formed on the catalyst surface upon exposure to CO₂, even if in a lower amount than under water-free conditions (Figure 3D; corresponding to Figure 3E at $t = 600$ s). This indicates a lower CO₂ storage capacity, possibly due to the competitive adsorption of H₂O onto the alkaline sites. CO₂ displays a more acidic behavior than water, and its adsorption on the alkaline site is favored with respect to water. However, H₂O has a higher partial pressure than CO₂ and this favors the competition of water during the adsorption process.

During the hydrogenation phase, the removal of carbonates from the surface appears slower than in the absence of water (Figure 3E; $t > 900$ s), and minor residual carbonates are left on the catalyst surface at the end (Figure 3F).

Figure 3H shows the integrated intensity of the adsorbed carbonate bands when CO₂ is adsorbed before and after H₂O

admission (violet and light blue traces, respectively). Inspection of the figure shows that water addition after CO₂ adsorption induces a significant drop in the carbonate band intensity (light blue trace, $t > 900$ s). This indicates that the presence of water rapidly displaces the adsorbed carbonates in the absence of CO₂ partial pressure. At variance, when the DFM is exposed to water before CO₂ (Figure 3H, purple), the amount of adsorbed carbonates is unaffected and very similar to that observed in the case of CO₂ adsorption on the clean DFM surface (Figure 3H; light blue trace at $t = 700$ s). Accordingly, the amounts of carbonates adsorbed at the end of the two adsorption sequences are very different, as can be seen from Figure 3G (corresponding to $t = 1500$ s in Figure 3H). In any case, upon H₂ admission, the carbonates are almost completely removed, although in both cases residual carbonates are left on the DFM surface (Figure 3I), in a similar way to that observed in the case of the cofeeding tests (Figure 3F), suggesting that in the presence of water carbonates are more difficult to hydrogenate and/or more strongly bound on the DFM.

3.4. O₂ Effect. The results obtained in the presence of O₂ during the CO₂ adsorption step are shown in Figure 4. When

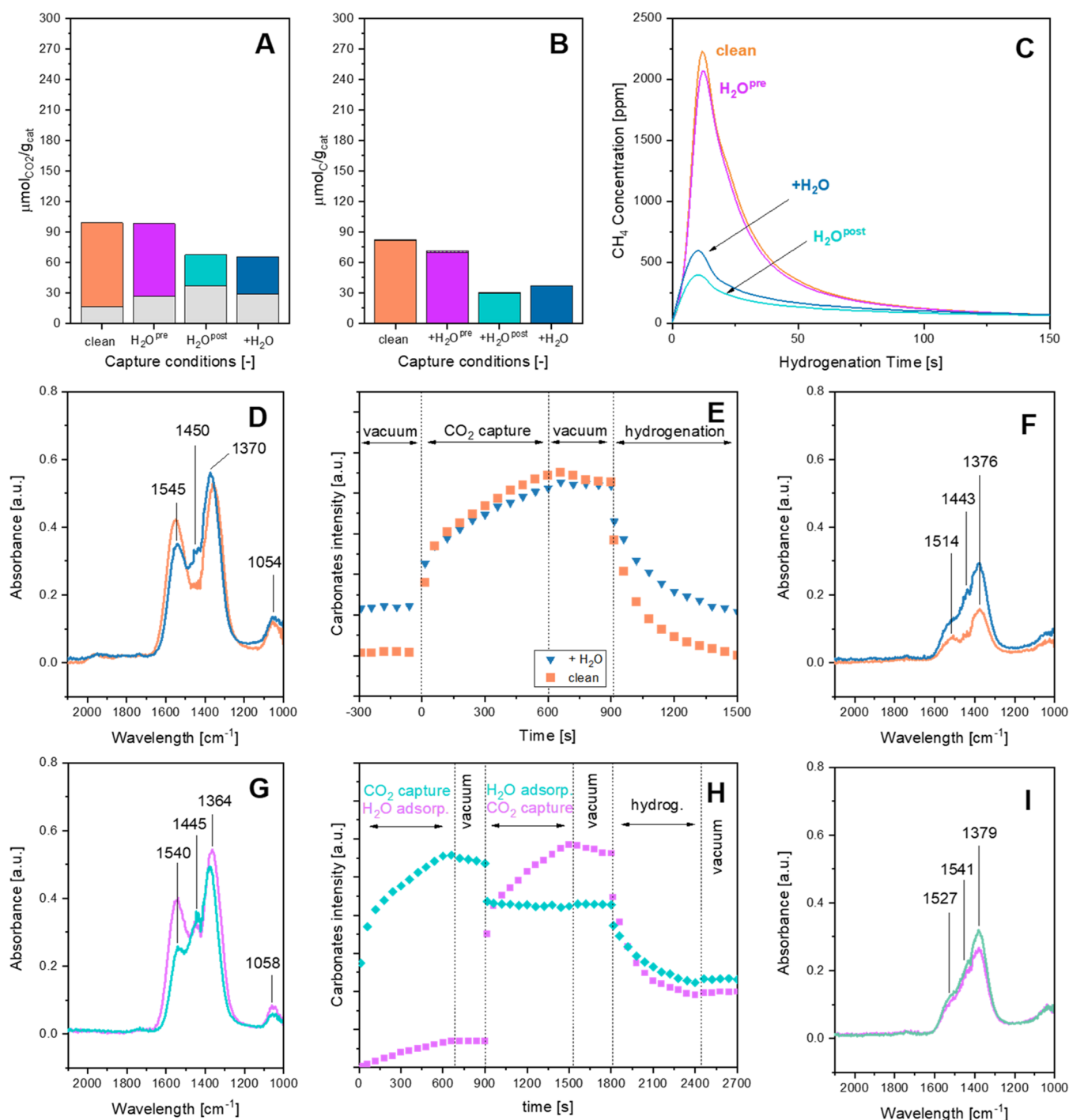


Figure 5. Effect of H_2O presence on CO_2 capture/methanation cycles by microreactor experiments (A–C) and effect of H_2O by in situ FT-IR (D–I) at a fixed temperature of $350\text{ }^\circ\text{C}$ on the Ru–Ba DFM. (A) Total CO_2 adsorbed during the capture step (total height), composed by a fraction that is hydrogenated at the same temperature of adsorption (colored bar) and by a fraction evolved only during heating (gray portion); (B) CH_4 (solid) and CO (dashed) produced during the hydrogenation step; (C) CH_4 evolution during the first 300 s of the hydrogenation step of the third cycle; (D) spectra at the end of the capture step ($t = 600\text{ s}$ in panel (E)); (E) qualitative evolution of carbonate bands during capture/hydrogenation cycles in the reference case and with cofed H_2O during the capture step; (F) spectra at the end of the hydrogenation step ($t = 1500\text{ s}$ in panel (E)); (G) spectra at the end of the capture steps ($t = 1800\text{ s}$ in panel (H)); (H) qualitative evolution of carbonate bands during capture/hydrogenation cycles with the additional H_2O adsorption step; (I) spectra at the end of the hydrogenation step ($t = 2400\text{ s}$ in panel (H)). Operating conditions, microreactor: adsorption: 1% $\text{CO}_2/2.5\%$ $\text{H}_2\text{O}/\text{He}$, 10 min; hydrogenation: 4% H_2/He , 10 min. Operating conditions, FT-IR: adsorption: 1 mbar $\text{CO}_2/25\text{ mbar}$ H_2O , 10 min; hydrogenation: 40 mbar H_2 , 10 min.

O_2 is present together with CO_2 during the adsorption phase, it causes a slight decrease in the CO_2 adsorption capacity (Figure 4A). In the FT-IR spectra (Figure 4D), the carbonate bands show a lower intensity due to the presence of oxygen

and the carbonyl species are no more observed, as previously reported.¹⁶ In particular, the trend in the carbonate intensity in Figure 4E ($t = 0\text{--}600\text{ s}$) indicates that at the beginning of the adsorption step the amount of adsorbed carbonates is the same

regardless of the O_2 presence. However, as the adsorption phase proceeds, the carbonate intensity grows more rapidly in the absence of O_2 , and the spectra at the end of the adsorption step (Figure 4D) show higher bands of the carbonates in the absence of O_2 (orange trace), especially in the case of the band at 1599 cm^{-1} . Of note, the formation of the broad negative band in the region of $2000\text{--}1800\text{ cm}^{-1}$ in the spectrum measured in the presence of oxygen is due to the displacement, upon O_2 exposure, of residual carbonyl species initially present on the surface.

This result suggests that also the adsorption on the alkaline sites can be affected to some extent by the presence of O_2 , which hinders the buildup of carbonates as the adsorption time proceeds. In addition, during the vacuum purge after the adsorption step (Figure 4E; $t = 600\text{--}900\text{ s}$), a faster decrease of carbonate bands is observed if the CO_2 adsorption is carried out in the presence of O_2 , possibly indicating that the carbonates adsorbed in the presence of O_2 are more weakly held on the DFM surface.

During the hydrogenation step, the selectivity toward methane is higher, as less CO is observed at the reactor outlet (Figure 4B). This is likely arising from the lack of contribution coming from CO adsorbed on Ru sites, which is desorbed fast at the beginning of the hydrogenation step in the absence of oxygen. The evolution of CH_4 in the gas phase is lower at the beginning of the H_2 pulse after the adsorption step in the presence of O_2 (Figure 4C), possibly due to the additional step of Ru reduction to its metallic state.¹⁸ By comparing the carbonate intensity during the hydrogenation step (Figure 4E; $t = 900\text{--}1500\text{ s}$), a very fast initial decrease is observed when the CO_2 adsorption is carried out in the presence of O_2 , but at the end of the corresponding hydrogenation step, residual carbonates and carbonyls are still present on the DFM surface (Figure 4F).

By coupling the results of the gas and surface analysis, it seems that in the presence of oxygen during the adsorption step, the subsequent hydrogenation occurs with a fast initial CO_2 desorption—possibly triggered by the temperature increase coming from Ru reduction—and the CO_2 is then slowly converted into methane along the catalyst bed. In fact, CO_2 was also detected during microreactor experiments at the beginning of the hydrogenation step during cycles in the presence of O_2 , adding up to $10\text{ }\mu\text{mol/g}$. At variance, in the absence of O_2 , the integral amount of CO_2 desorbed during the hydrogenation step is lower than $5\text{ }\mu\text{mol/g}$ (shown in Figure S3 of the Supporting Information).

When water and oxygen are present simultaneously (purple bars/evolution profile in Figure 4A–C), the effect of water prevails, with an important reduction in the CO_2 storage capacity. In fact, the amount of adsorbed CO_2 /formed products appears very similar to that observed when only water is present in the feed (compare the purple bar/profile in Figure 4A–C with the blue bar/profile in the corresponding Figure 3A–C).

3.5. Comparison with Ba-Based DFM. The effect of H_2O presence was also investigated for the Ba-based DFM under the same experimental conditions adopted in the case of the K-based sample (refer to Figures S1 and S4 of the Supporting Information for the experimental procedures), and the results are shown in Figure 5. In the absence of water (“clean conditions”), the Ba-based DFM adsorbs lower amounts of CO_2 if compared to the K-based sample (compare Figure 5A with 3A), and the resulting carbonates are more

difficult to hydrogenate completely with respect to the carbonates formed on other storage components such as K and Na.^{9,19} This results in a larger fraction of carbonates left on the DFM surface at the end of the hydrogenation phase.

The effect of water has been investigated, and the results of microreactor experiments are compared in Figure 5A–C with those obtained in the absence of water. When water is present during or after the adsorption of CO_2 (“+ H_2O ” and “ H_2O^{post} ”, respectively), the amount of C-based products evolving from the DFM during the hydrogenation cycle and the final heating to $500\text{ }^\circ\text{C}$ is lower compared to the test performed in the absence of water (total heights; Figure 5A). At variance, when H_2O is fed before CO_2 to prehydrate the DFM, the total amount of C-based species is similar to the clean test (total heights; Figure 5A). However, in the presence of preadsorbed water, the relative amounts of CO_2 hydrogenated during the cycle (Figure 5A, in color) decrease with respect to those evolved during the final heating in H_2 (Figure 5A, in gray). In fact, when the Ba-based DFM is exposed to water, regardless of the feeding order, an increase in the stable fraction of the carbonates is observed, resulting in a lower production of CH_4 during the hydrogenation step in isothermal conditions (Figure 5B). As a matter of fact, comparing the CH_4 evolution in the gas phase during the isothermal hydrogenation step (Figure 5C), it appears that when water is present during or after the adsorption of CO_2 , CH_4 formation is strongly affected, while little to no difference is observed when the sample is prehydrated.

The concentration in the effluents during the “+ H_2O^{pre} ” and “+ H_2O^{post} ” experiments is shown also in the case of the Ba-based DFM in the Supporting Information, Figure S7. As previously observed in the case of the K-based DFM, also in this case when water is fed over the CO_2 -saturated DFM, CO_2 is released as a result of water adsorption and vice versa, highlighting also in this case the competitive adsorption of CO_2 and H_2O for the same BaO sites.

To get more insights into the role of water during the capture step on the Ba-based DFM, the same FT-IR tests carried out in the case of the K-based DFM were replicated on the Ba-based sample and the results are shown in Figure 5D–I. By comparing the carbonate integrated intensity during the isothermal cycle when the capture is carried out in the absence and presence of water vapor (Figure 5E; $t = 0\text{--}600\text{ s}$), it can be observed that during the capture step, similar intensity of the carbonate species is apparent on Ba, regardless of the presence of H_2O . As revealed in Figure 5D, bidentate carbonates (evidenced by the features at 1545 , 1370 , 1054 cm^{-1} ^{132,33}) are the main species present at the end of the adsorption step in the absence of water. Of note, differently from the case of K where the two main features at ca. 1600 and ca. 1320 cm^{-1} are symmetrical, in the case of Ba the feature at lower wavelength (i.e., 1370 cm^{-1}) appears more pronounced. This may indicate the formation of also ionic carbonates adsorbed on the Ba phase overlapping the band related to bidentate carbonates.³⁴ In line with this hypothesis, when the adsorption of CO_2 is performed in the presence of water vapor, the bidentate carbonate bands are still clearly visible but the asymmetry between the two main bands becomes more pronounced, with the envelope at 1545 cm^{-1} losing intensity while the one at 1370 cm^{-1} increases. Furthermore, an additional feature at 1450 cm^{-1} becomes evident in the presence of water vapor. In fact, the increase of both bands at 1370 and 1450 cm^{-1} at the expense of the band at 1545 cm^{-1} is likely connected to the

transformation of bidentate carbonates into ionic carbonates, in analogy to what has been observed on similar catalyst formulations for different applications.³⁴

During the hydrogenation step of the cycle (Figure 5E; $t = 900\text{--}1500\text{ s}$), the carbonates adsorbed in the presence of water appear more difficult to hydrogenate, and this results in a higher integrated intensity of carbonates on the DFM at the end of the hydrogenation step (Figure 5E, $t = 1500\text{ s}$; corresponding spectra in Figure 5F). This can be attributed to the higher stability of the ionic carbonates formed upon water exposure.

When water is fed after CO_2 (Figure 5H, light blue diamonds), the carbonate intensity shows a steep decrease upon water admission, and also in this case, the band at 1445 cm^{-1} is visible at the end of the adsorption step (Figure 5G, light blue line), indicating the presence of ionic carbonates.

In conclusion, H_2O can be competitively adsorbed on Ba sites, resulting in a decrease of the available CO_2 adsorption sites for the cyclic capture and methanation. Furthermore, the nature of the surface carbonate changes when exposed to water, leading to the formation of more stable ionic carbonates on the DFM surface. This behavior—even if to a much lower extent—was also observed in the case of the K-based DFM, and indicates that sturdy carbonates can form on the DFM in the presence of water. This could lead to the progressive accumulation of stable carbonates on the DFM upon cycling, progressively eroding CO_2 adsorption sites and ultimately resulting in a loss of the CO_2 adsorption capacity of the sample.

4. CONCLUSIONS

In this work, we have investigated the reactivity of K-based dual-function materials based on ruthenium in the cyclic CO_2 capture and methanation. The effect of different operating conditions (T , P_{H_2} , water, and O_2 presence) on the catalytic performances has been addressed by means of microreactor experiment and FT-IR spectroscopy.

It has been found that in the $250\text{--}350\text{ }^\circ\text{C}$ temperature range CO_2 is rapidly adsorbed as bidentate carbonate onto the DFM surface. Up to $270\text{ }\mu\text{mol}_{\text{CO}_2}/\text{g}_{\text{cat}}$ can be adsorbed at $250\text{ }^\circ\text{C}$. However, upon adsorption at the lowest investigated temperatures, the stored carbonates can be hardly reduced, unless upon heating at higher temperatures. At variance, at temperatures near $350\text{--}400\text{ }^\circ\text{C}$, the amount of adsorbed CO_2 is lower, but the stored carbonates can be almost entirely reduced at the same temperature of adsorption. Temperature increase also favors the rate of carbonate hydrogenation due to kinetic reasons.

Increasing the H_2 partial pressure favors the rate of the reduction of the adsorbed species to methane and consequently the regeneration of the sorbent material. The presence of water during the CO_2 adsorption step has a dual effect: on one hand, it competes with CO_2 for the adsorption sites, lowering the overall storage capacity of the DFM; on the other hand, it can change the nature of the adsorbed carbonates, increasing their ionic behavior and their stability.

The presence of O_2 during the adsorption phase reduces the amount of CO_2 adsorbed sites by removing reduced Ru surfaces (where CO can be adsorbed) and possibly reduces the bidentate carbonate intensity due to the water that is formed as a result of the Ru oxide reduction.

Finally, a comparison with an analogous Ba-containing Ru-based DFM sample under selected experimental conditions has also been carried out. Under the same experimental conditions, the Ba-based material shows a lower CO_2 adsorption capacity and the formation of more stable and refractive carbonates. Like the K-based sample, water also negatively impacts the behavior of the Ba-containing material and on the latter the effect was even more pronounced.

■ ASSOCIATED CONTENT

Supporting Information

The Supporting Information is available free of charge at <https://pubs.acs.org/doi/10.1021/acs.energyfuels.3c00443>.

Additional experimental details; a complete microreactor CO_2 capture/reduction cycle with the indication of the gas concentration signals used for the quantification of adsorbed CO_2 and evolved C-products; quantitative results from microreactor experiments given in table format; and gas-phase composition during microreactor experiments on the effect of water (PDF)

■ AUTHOR INFORMATION

Corresponding Author

Luca Lietti — Dipartimento di Energia, Politecnico Di Milano, Milano 20156, Italy; orcid.org/0000-0002-2888-9708; Email: luca.lietti@polimi.it

Authors

Alessandro Porta — Dipartimento di Energia, Politecnico Di Milano, Milano 20156, Italy; orcid.org/0000-0002-1445-907X

Roberto Matarrese — Dipartimento di Energia, Politecnico Di Milano, Milano 20156, Italy; orcid.org/0000-0002-3499-6614

Carlo Giorgio Visconti — Dipartimento di Energia, Politecnico Di Milano, Milano 20156, Italy; orcid.org/0000-0001-5205-982X

Complete contact information is available at:

<https://pubs.acs.org/doi/10.1021/acs.energyfuels.3c00443>

Notes

The authors declare no competing financial interest.

■ REFERENCES

- (1) Duyar, M. S.; Wang, S.; Arellano-Treviño, M. A.; Farrauto, R. J. CO_2 Utilization with a Novel Dual Function Material (DFM) for Capture and Catalytic Conversion to Synthetic Natural Gas: An Update. *J. CO₂ Util.* **2016**, *15*, 65–71.
- (2) Farrauto, R. J.; Duyar, M. S.; Park, A. A. Methods, Systems and Materials for Capturing Carbon Dioxide and Converting It to a Chemical Product. WO Patent WO2016/007825A1, 2016.
- (3) Bravo, P. M.; Debecker, D. P. Combining CO_2 Capture and Catalytic Conversion to Methane. *Waste Disposal Sustainable Energy* **2019**, *1*, 53–65.
- (4) Tsiotsias, A. I.; Charisiou, N. D.; Yentekakis, I. V.; Goula, M. A. The Role of Alkali and Alkaline Earth Metals in the CO_2 Methanation Reaction and the Combined Capture and Methanation of CO_2 . *Catalysts* **2020**, *10*, No. 812.
- (5) Chen, J.; Xu, Y.; Liao, P.; Wang, H.; Zhou, H. Recent Progress in Integrated CO_2 Capture and Conversion Process Using Dual Function Materials: A State-of-the-Art Review. *Carbon Capture Sci. Technol.* **2022**, *4*, No. 100052.

- (6) Omodolor, I. S.; Otor, H. O.; Andonegui, J. A.; Allen, B. J.; Alba-Rubio, A. C. Dual-Function Materials for CO₂ Capture and Conversion: A Review. *Ind. Eng. Chem. Res.* **2020**, *59*, 17612–17631.
- (7) Merkouri, L.-P.; Reina, T. R.; Duyar, M. S. Closing the Carbon Cycle with Dual Function Materials. *Energy Fuels* **2021**, *35*, 19859–19880.
- (8) Proaño, L.; Tello, E.; Arellano-Trevino, M. A.; Wang, S.; Farrauto, R. J.; Cobo, M. In-Situ DRIFTS Study of Two-Step CO₂ Capture and Catalytic Methanation over Ru/Na₂O/Al₂O₃ Dual Functional Material. *Appl. Surf. Sci.* **2019**, *479*, 25–30.
- (9) Porta, A.; Matarrese, R.; Visconti, C. G.; Castoldi, L.; Lietti, L. Storage Material Effects on the Performance of Ru-Based CO₂ Capture and Methanation Dual Functioning Materials. *Ind. Eng. Chem. Res.* **2021**, *60*, 6706–6718.
- (10) Jeong-Potter, C.; Porta, A.; Matarrese, R.; Visconti, C. G.; Lietti, L.; Farrauto, R. Aging Study of Low Ru Loading Dual Function Materials (DFM) for Combined Power Plant Effluent CO₂ Capture and Methanation. *Appl. Catal., B* **2022**, *310*, No. 121294.
- (11) Porta, A.; Visconti, C. G.; Castoldi, L.; Matarrese, R.; Jeong-Potter, C.; Farrauto, R.; Lietti, L. Ru-Ba Synergistic Effect in Dual Functioning Materials for Cyclic CO₂ Capture and Methanation. *Appl. Catal., B* **2021**, *283*, No. 119654.
- (12) Bermejo-López, A.; Pereda-Ayo, B.; González-Marcos, J. A.; González-Velasco, J. R. Mechanism of the CO₂ Storage and in Situ Hydrogenation to CH₄. Temperature and Adsorbent Loading Effects over Ru-CaO/Al₂O₃ and Ru-Na₂CO₃/Al₂O₃ Catalysts. *Appl. Catal., B* **2019**, *256*, No. 117845.
- (13) Park, S. J.; Wang, X.; Ball, M. R.; Proano, L.; Wu, Z.; Jones, C. W. CO₂ Methanation Reaction Pathways over Unpromoted and NaNO₃-Promoted Ru/Al₂O₃ Catalysts. *Catal. Sci. Technol.* **2022**, *12*, 4637–4652.
- (14) Wang, X.; Shi, H.; Szanyi, J. Controlling Selectivities in CO₂ Reduction through Mechanistic Understanding. *Nat. Commun.* **2017**, *8*, No. 513.
- (15) Falbo, L.; Visconti, C. G.; Lietti, L.; Szanyi, J. The Effect of CO on CO₂ Methanation over Ru/Al₂O₃ Catalysts: A Combined Steady-State Reactivity and Transient DRIFT Spectroscopy Study. *Appl. Catal., B* **2019**, *256*, No. 117791.
- (16) Proaño, L.; Arellano-Treviño, M. A.; Farrauto, R. J.; Figueredo, M.; Jeong-Potter, C.; Cobo, M. Mechanistic Assessment of Dual Function Materials, Composed of Ru-Ni, Na₂O/Al₂O₃ and Pt-Ni, Na₂O/Al₂O₃, for CO₂ Capture and Methanation by in-Situ DRIFTS. *Appl. Surf. Sci.* **2020**, *533*, No. 147469.
- (17) Bermejo-López, A.; Pereda-Ayo, B.; González-Marcos, J. A.; González-Velasco, J. R. Alternate Cycles of CO₂ Storage and in Situ Hydrogenation to CH₄ on Ni-Na₂CO₃/Al₂O₃: Influence of Promoter Addition and Calcination Temperature. *Sustain. Sustainable Energy Fuels* **2021**, *5*, 1194–1210.
- (18) Wang, S.; Schunk, E. T.; Mahajan, H.; Farrauto, R. J. The Role of Ruthenium in CO₂ Capture and Catalytic Conversion to Fuel by Dual Function Materials (DFM). *Catalysts* **2017**, *7*, No. 88.
- (19) Arellano-Treviño, M. A.; He, Z.; Libby, M. C.; Farrauto, R. J. Catalysts and Adsorbents for CO₂ Capture and Conversion with Dual Function Materials: Limitations of Ni-Containing DFMs for Flue Gas Applications. *J. CO₂ Util.* **2019**, *31*, 143–151.
- (20) Arellano-Treviño, M. A.; Kanani, N.; Jeong-Potter, C. W.; Farrauto, R. J. Bimetallic Catalysts for CO₂ Capture and Hydrogenation at Simulated Flue Gas Conditions. *Chem. Eng. J.* **2019**, *375*, No. 121953.
- (21) Jeong-Potter, C.; Abdallah, M.; Sanderson, C.; Goldman, M.; Gupta, R.; Farrauto, R. Dual Function Materials (Ru+Na₂O/Al₂O₃) for Direct Air Capture of CO₂ and in Situ Catalytic Methanation: The Impact of Realistic Ambient Conditions. *Appl. Catal., B* **2022**, *307*, No. 120990.
- (22) Bermejo-López, A.; Pereda-Ayo, B.; González-Marcos, J. A.; González-Velasco, J. R. Ni Loading Effects on Dual Function Materials for Capture and In-Situ Conversion of CO₂ to CH₄ Using CaO or Na₂CO₃. *J. CO₂ Util.* **2019**, *34*, 576–587.
- (23) Frontera, P.; Macario, A.; Ferraro, M.; Antonucci, P. Supported Catalysts for CO₂ Methanation: A Review. *Catalysts* **2017**, *7*, No. 59.
- (24) Vogt, C.; Monai, M.; Kramer, G. J.; Weckhuysen, B. M. The Renaissance of the Sabatier Reaction and Its Applications on Earth and in Space. *Nat. Catal.* **2019**, *2*, 188–197.
- (25) Prinetto, F.; Manzoli, M.; Morandi, S.; Frola, F.; Ghiotti, G.; Castoldi, L.; Lietti, L.; Forzatti, P. Pt-K/Al₂O₃ NSR Catalysts: Characterization of Morphological, Structural and Surface Properties. *J. Phys. Chem. C* **2010**, *114*, 1127–1138.
- (26) Montanari, T.; Castoldi, L.; Lietti, L.; Busca, G. Basic Catalysis and Catalysis Assisted by Basicity: FT-IR and TPD Characterization of Potassium-Doped Alumina. *Appl. Catal., A* **2011**, *400*, 61–69.
- (27) Wang, X.; Hong, Y.; Shi, H.; Szanyi, J. Kinetic Modeling and Transient DRIFTS-MS Studies of CO₂ Methanation over Ru/Al₂O₃ Catalysts. *J. Catal.* **2016**, *343*, 185–195.
- (28) Panagiotopoulou, P.; Verykios, X. E. Mechanistic Study of the Selective Methanation of CO over Ru/TiO₂ Catalysts: Effect of Metal Crystallite Size on the Nature of Active Surface Species and Reaction Pathways. *J. Phys. Chem. C* **2017**, *121*, S058–S068.
- (29) Jeong-Potter, C.; Farrauto, R. Feasibility Study of Combining Direct Air Capture of CO₂ and Methanation at Isothermal Conditions with Dual Function Materials. *Appl. Catal., B* **2021**, *282*, No. 119416.
- (30) Koschany, F.; Schlereth, D.; Hinrichsen, O. On the Kinetics of the Methanation of Carbon Dioxide on Coprecipitated NiAl(O)_x. *Appl. Catal., B* **2016**, *181*, 504–516.
- (31) Falbo, L.; Martinelli, M.; Visconti, C. G.; Lietti, L.; Bassano, C.; Deiana, P. Kinetics of CO₂ Methanation on a Ru-Based Catalyst at Process Conditions Relevant for Power-to-Gas Applications. *Appl. Catal., B* **2018**, *225*, 354–363.
- (32) Frola, F.; Prinetto, F.; Ghiotti, G.; Castoldi, L.; Nova, I.; Lietti, L.; Forzatti, P. Combined in Situ FT-IR and TRM Analysis of the NO_x Storage Properties of Pt-Ba/Al₂O₃ LNT Catalysts. *Catal. Today* **2007**, *126*, 81–89.
- (33) Frola, F.; Manzoli, M.; Prinetto, F.; Ghiotti, G.; Castoldi, L.; Lietti, L. Pt-Ba/Al₂O₃ NSR Catalysts at Different Ba Loading: Characterization of Morphological, Structural, and Surface Properties. *J. Phys. Chem. C* **2008**, *112*, 12869–12878.
- (34) Morandi, S.; Prinetto, F.; Ghiotti, G.; Castoldi, L.; Lietti, L.; Forzatti, P.; Daturi, M.; Blasin-Aubé, V. The Influence of CO₂ and H₂O on the Storage Properties of Pt-Ba/Al₂O₃ LNT Catalyst Studied by FT-IR Spectroscopy and Transient Microreactor Experiments. *Catal. Today* **2014**, *231*, 116–124.